Original Article

Abdominal virtual non-contrast images derived from energy spectrum CT to evaluate chemotherapy-related fatty liver disease

Mengyuan Jing[1,2,3,4#], Jiachen Sun[1,2,3,4#], Huaze Xi[1,2,3,4], Zhuoheng Liu[5], Shuai Zhang[5], Liangna Deng[1,2,3,4], Tao Han[1,2,3,4], Bin Zhang[1,2,3,4], Xiaoqiang Lin[1,2,3,4], Junlin Zhou[1,2,3,4]

[1]Department of Radiology, Lanzhou University Second Hospital, Lanzhou, China; [2]Second Clinical School, Lanzhou University, Lanzhou, China; [3]Key Laboratory of Medical Imaging of Gansu Province, Lanzhou, China; [4]Gansu International Scientific and Technological Cooperation Base of Medical Imaging Artificial Intelligence, Lanzhou, China; [5]Computed Tomography Research Center, GE Healthcare China, Beijing, China

Contributions: (I) Conception and design: M Jing, J Sun; (II) Administrative support: J Zhou; (III) Provision of study materials or patients: M Jing, H Xi, L Deng, T Han; (IV) Collection and assembly of data: J Sun, B Zhang, X Lin; (V) Data analysis and interpretation: Z Liu, S Zhang; (VI) Manuscript writing: All authors; (VII) Final approval of manuscript: All authors.

[#]These authors contributed equally to this work and should be considered as co-first authors.

Correspondence to: Junlin Zhou, MD. Department of Radiology, Lanzhou University Second Hospital, Cuiyingmen No. 82, Chengguan District, Lanzhou 730030, China. Email: ery_zhoujl@lzu.edu.cn.

Background: Chemotherapy-related fatty liver disease (CRFLD) is an important evaluation in patients undergoing computed tomography (CT) for cancer follow-up. This study set out to explore the feasibility of using abdominal virtual non-contrast (VNC) images derived from energy spectrum CT to evaluate CRFLD and reduce the radiation dose.

Methods: A total of 160 eligible consecutive patients who underwent energy spectrum CT at Lanzhou University Second Hospital between June 2020 and July 2021 were retrospectively enrolled. The average CT attenuation values of the liver and spleen and the liver-to-spleen ratio (LSR) were measured by two independent blinded radiologists on true non-contrast (TNC) images and three types of VNC image. The diagnostic performance of the LSR for CRFLD, image quality, and diagnostic confidence were compared between the two types of imaging.

Results: The average CT attenuation values of the liver and spleen were significantly lower on VNC images than on TNC images ($P<0.05$), whereas the LSR showed good agreement between the two ($P>0.05$). The average CT attenuation values of the liver and the LSR measured on the TNC and three types of VNC image were significantly lower in patients with CRFLD than in those without CRFLD ($P<0.001$). The area under the curve (AUC) values of the LSR for the diagnosis of CRFLD calculated on TNC and three types of VNC image were 0.870 (95% CI: 0.808–0.918), 0.852 (95% CI: 0.787–0.903), 0.819 (95% CI: 0.750–0.875), and 0.851 (95% CI: 0.786–0.902), respectively. The DeLong test confirmed the consistency of TNC and VNC images of diagnostic efficacy ($P>0.05$). There were no significant differences in image quality or diagnostic confidence between the TNC and three types of VNC image ($P>0.05$). When VNC imaging was applied, the radiation dose was reduced by approximately 25.0%.

Conclusions: VNC imaging could become a reliable alternative to TNC imaging for the clinical evaluation of patients with CRFLD and could reduce the radiation dose by up to 25%.

Keywords: Energy spectrum computed tomography; chemotherapy-related fatty liver; virtual non-contrast (VNC); computed tomography attenuation value

Submitted Jul 15, 2022. Accepted for publication Nov 24, 2022. Published online Jan 02, 2023.
doi: 10.21037/qims-22-742
View this article at: https://dx.doi.org/10.21037/qims-22-742

Introduction

The prevalence of non-alcoholic fatty liver disease (NAFLD) has been increasing rapidly in Asia, reaching 33.9% in 2015–2017 (1,2). Various factors are associated with NAFLD, including obesity and hyperlipidemia, parenteral nutrition, and the use of steroids and chemotherapy drugs (3,4). Chemotherapy-related fatty liver disease (CRFLD), one type of NAFLD, is a chronic but reversible disease associated with continuous chemotherapy in which drugs accumulate in the liver, resulting in excess phospholipids in the cells (5). Owing to the widespread use of chemotherapeutics in patients with cancer and their increased risk of postoperative death and liver failure (6,7), CRFLD monitoring during chemotherapy is crucial to improving patient prognosis.

Although liver biopsy is considered the gold reference standard for diagnosing and classifying fatty liver (8), it carries the risk of complications such as bleeding (9). Noninvasive imaging techniques can also detect fatty liver disease and help diagnose steatosis (10-13). Magnetic resonance imaging (MRI) is considered to have good diagnostic performance, but its application is limited by the high cost of examination and numerous clinical contraindications, such as the presence of metal foreign bodies and claustrophobia, which prevent patients from undergoing MRI examination (14). Ultrasonography is cost-effective; however, the interpretation of its findings depends on subjective evaluation by a physician. In clinical practice, computed tomography (CT) carries the advantages of having a low price, a short scanning time, and fewer contraindications than other imaging techniques. In addition, it is the most widely used image examination method and is often applied clinically for tumor staging and patient follow-up (15). For patients with cancer, CT can simultaneously be applied to follow up on cancer response to therapy by observing the volume change of the lesion before and after chemotherapy and to evaluate fatty liver, thereby optimizing the clinician's time and reducing the financial resources required.

In clinical practice, non-enhanced CT is the most popularly used approach to identify fatty liver disease. It determines the measurement based on liver attenuation (13) and derives the liver-to-spleen ratio (LSR; LSR = CT value liver/CT value spleen ratio), which is regarded as a convenient and widely available measure of liver fat (16). The liver fat fraction from dual-energy CT has also been proposed for non-invasive diagnosis of fatty liver (17). However, excessive radiation doses are a major concern with CT use (18). For patients with cancer, non-contrast combined with contrast CT is a common scanning modality that can prevent the omission of metastatic lesions, but patients usually receive higher radiation doses compared to non-ionizing imaging techniques, such as MRI and ultrasonography. Virtual non-contrast (VNC) imaging, based on the energy spectrum CT multimaterial decomposition algorithm, mitigates radiation dose exposure (19). It does this by using technology that can accomplish iodine removal and the subsequent addition of blood after image acquisition through the use of postprocessing material separation techniques (20). Therefore, VNC imaging can serve as an appropriate substitute for true non-contrast (TNC) imaging, reducing the scan time and radiation dose required (21-23).

In this study, we hypothesized that VNC imaging would demonstrate similar diagnostic capabilities as TNC imaging. We attempted to demonstrate that VNC technology can be applied in place of TNC imaging in abdominal imaging for the evaluation of CRFLD and help to clinically simplify the scanning process, shorten the scan time, and reduce the radiation dose. We present the following article in accordance with the STARD reporting checklist (available at https://qims.amegroups.com/article/view/10.21037/qims-22-742/rc).

Methods

Study design and population

The study was conducted in accordance with the Declaration of Helsinki (as revised in 2013). The Ethics Committee of Lanzhou University Second Hospital approved this study (No. 2020A-284), and the requirement to obtain individual consent for this retrospective analysis was waived.

We retrospectively screened 277 patients at Lanzhou University Second Hospital who were diagnosed with various types of cancer and underwent dual-energy CT of the abdomen following at least two cycles of chemotherapy between June 2020 and July 2021. Patients were excluded if: (I) the interval between their last chemotherapy cycle and CT examination was >6 weeks (n=41); (II) the interval between abdominal energy spectrum CT, MRI, and ultrasonography was >2 weeks (n=10); (III) they had no MRI or ultrasonographic images (n=11); (IV) they had a history of fatty liver, liver disease, liver tumors, or substantial alcohol intake before treatment (n=28); (V) they had a

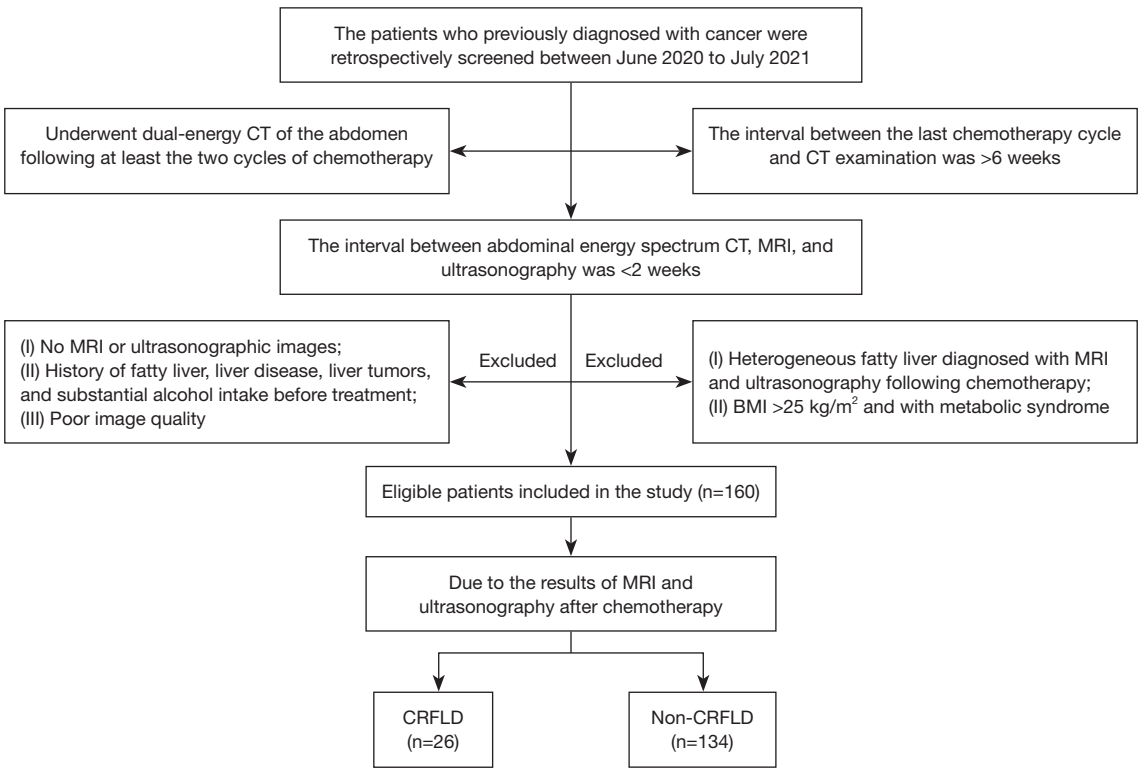

Figure 1 The screening process for patients with and without CRFLD. CT, computed tomography; BMI, body mass index; MRI, magnetic resonance imaging; CRFLD, chemotherapy-related fatty liver disease.

body mass index (BMI) >25 kg/m^2 (n=12); (VI) they had metabolic syndrome (n=1); (VII) they had heterogeneous fatty liver diagnosed with MRI and ultrasonography following chemotherapy (n=9); or (VIII) their data had poor image quality (n=5). Finally, 160 patients that met the inclusion and exclusion criteria were enrolled in the study.

Based on the MRI DIXON sequence in-phase/opposed-phase and ultrasound diagnostic results following chemotherapy, the patients were divided into the non-CRFLD (n=134) and CRFLD (n=26) groups. Comprising patients with cancer who did not have fatty liver disease after chemotherapy, the non-CRFLD group served as a control group. In the CRFLD group, there were 9 patients with gastric cancer, 5 patients with lung cancer, 5 patients with colorectal cancer, 5 patients with breast cancer, 1 patient with ovarian cancer, and 1 patient with esophageal cancer. The screening and grouping processes are shown in *Figure 1*.

Acquisition of CT images

Abdominal dual-energy CT was performed using a 256-row CT scanner (Revolution CT, GE Healthcare, Milwaukee, WI, USA). The scan range was from the upper edge of the liver to the lower edge of the pubic symphysis. The scan parameters were as follows: scanning field of view, 50 cm; display field of view, 24; matrix, 512×512; rapid switching between tube voltages, 80 and 140 kVp; tube current, 405 mA; kernel, standard; adaptive statistical iterative reconstruction Veo, 50%; rotation time, 0.5 s; helical pitch, 0.992:1; and slice thickness, 1.25 mm. Enhanced scanning was performed using a high-pressure dual-cylinder syringe (Bayer HealthCare AG, Germany), and iohexol (1 mL/kg) was injected through the median cubital vein at a rate of 4–4.5 mL/s. After injection of the contrast agent, the arterial phase was scanned when the intelligent monitoring reached its peak, while the venous and delayed phases were scanned at 30 and 90 s, respectively.

Objective assessment

The abdominal CT images were analyzed using an Advanced Workstation 4.7 (AW4.7; GE Healthcare) by two radiologists. The first reviewer had 9 years of abdominal diagnostic

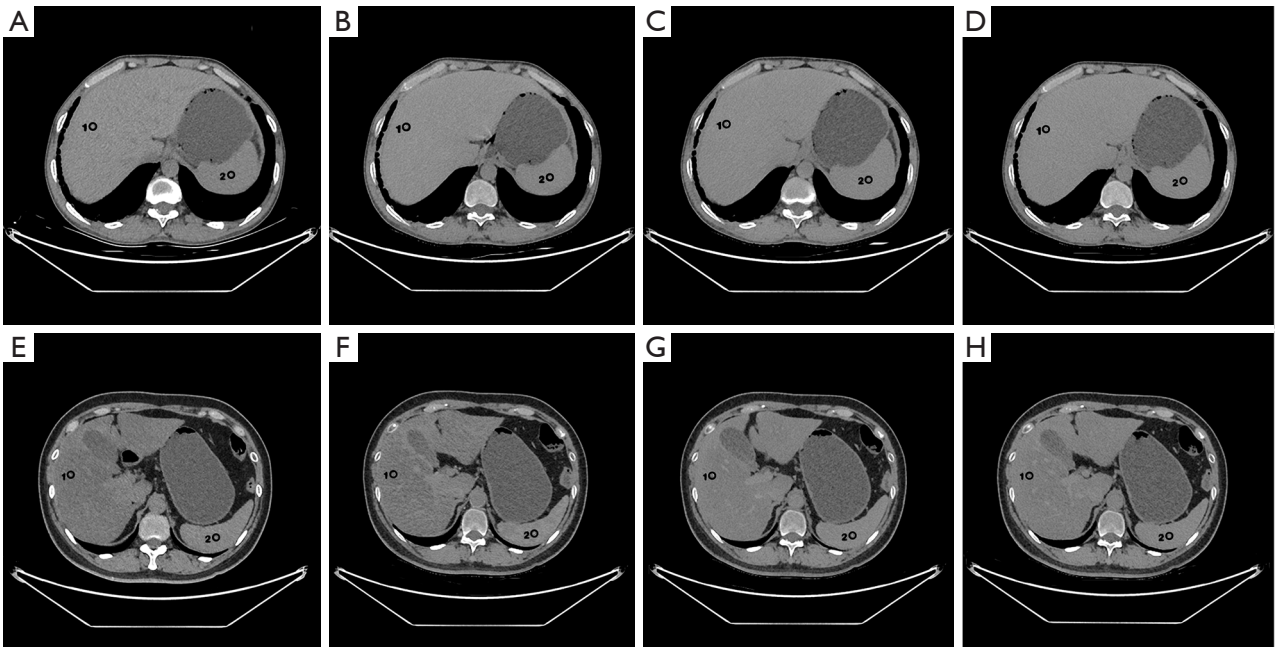

Figure 2 Measurement of the average CT attenuation values of the liver and spleen. (A) Measurement of the liver and spleen on a TNC image from the non-CRFLD group. (B) Measurement of the liver and spleen on a VNCa image from the non-CRFLD group. (C) Measurement of the liver and spleen on a VNCv image from the non-CRFLD group. (D) Measurement of the liver and spleen on a VNCd image from the non-CRFLD group. (E) Measurement of the liver and spleen on a TNC image from the CRFLD group. (F) Measurement of the liver and spleen on a VNCa image from the CRFLD group. (G) Measurement of the liver and spleen on a VNCv image from the CRFLD group. (H) Measurement of the liver and spleen on a VNCd image from the CRFLD group. CT, computed tomography; TNC, true non-contrast; CRFLD, chemotherapy-related fatty liver disease; VNCa, virtual non-contrast from the arterial phase; VNCv, virtual non-contrast from the venous phase; VNCd, virtual non-contrast from the delayed phase.

experience, and the second had 13 years of abdominal diagnostic experience. The reviewers were unaware of the patients' clinical information and diagnostic imaging results. In total, three CT parameters were evaluated: the CT attenuation values of the liver and spleen and the calculated LSR. The CT image analysis was performed as follows. First, VNC images of the arterial (VNCa), venous (VNCv), and delay (VNCd) phases were calculated using an AW4.7 workstation. Second, on the axial TNC images, the two reviewers independently drew regions of interest (ROIs) of 3 cm in diameter in 4/8 segments of the liver, avoiding the blood vessels and bile duct. At the same level as the liver, the two reviewers each drew an ROI in the center of the spleen. Third, all the ROIs from the TNC images were copied and pasted onto three corresponding VNC images. Finally, the average calculated from the measurement results of the two radiologists was taken as the final value. *Figure 2* shows the ROIs measured on the TNC and VNC images of patients with CRFLD and without CRFLD.

Since a difference of less than 10 Hounsfield units (HU) between VNC and TNC images can be ignored, and a difference of less than 5 HU can help to further validate the effect of VNC, we calculated the percentage of cases with differences of less than 5 HU and less than 10 HU between the TNC and three VNC attenuation values of the liver and spleen (24). Also, the receiver operating characteristic (ROC) curve was plotted to evaluate the performance of the LSR calculated on the TNC and three types of VNC image for diagnosing CRFLD.

Subjective assessment

To ensure the rigor of the evaluation, 1 month later, the two reviewers subjectively assessed the quality of the TNC and three types of VNC image using the following scale: 5= excellent; 4= good; 3= fair; 2= poor; and 1= unreadable (23). Further, based on differences in the visual attenuation of the liver relative to that of the spleen, the two reviewers

subjectively scored their diagnostic confidence (i.e., their confidence that they had correctly diagnosed CRFLD) with the TNC and three types of VNC image. Scores were assigned as follows: 5=100% confidence; 4=75% confidence; 3=50% confidence; 2=25% confidence; and 1=0% confidence. If the diagnostic results of the two radiologists were different, a more senior chief physician was asked to make the final diagnosis.

Radiation dose analysis

The dose length product (DLP), volume CT dose index (CTDIvol), and effective dose (ED) values were used to assess the possible dose that was spared by eliminating the unenhanced examination. The DLP and CTDIvol were presented in the dose report of the CT scan, and the ED was the product of the DLP multiplied by a conversion factor of 0.015 (25).

Statistical analysis

Continuous variables were expressed as median (interquartile range) or mean ± standard deviation. Classification variables were presented as frequency (percentage). Intra-/interclass correlation coefficients (ICCs) were used to calculate the consistency of all measurements or assessments between the two radiologists. Classification variables were analyzed using the chi-square test. The subjective assessment and the CT attenuation values of the liver and spleen and the LSR measured on the TNC images were compared to those measured on the three types of VNC image using the Wilcoxon signed-rank test and the paired *t*-test. Bland-Altman analysis was used to evaluate the measurement agreement of the LSR between the TNC and three types of VNC image. Differences in the CT attenuation values of the liver and spleen and the LSR between patients with and without CRFLD were calculated using the Wilcoxon Mann-Whitney U test or an independent *t*-test. The area under the ROC curve (AUC) value of the LSR from the TNC images was compared to those of the three types of VNC image using the DeLong test. All data were analyzed using SPSS 23.0 (IBM Corp. Armonk, NY, USA) and MedCalc 19.6 (MedCalc Software Ltd., Ostend, Belgium).

Results

Interobserver agreement

Excellent agreement was observed between the two radiologists in the measurements of all CT attenuation values of the liver and spleen (all ICC values >0.80; Table S1).

Comparison of TNC images and three types of VNC image

The average CT attenuation values of the liver on VNCa, VNCv, and VNCd images were 61.25 (57.00–65.70) HU, 62.30 (58.50–66.68) HU, and 61.70 (57.80–66.23) HU, respectively; all these values were significantly lower than those on the TNC images [63.00 (57.25–71.75) HU; P<0.001]. Additionally, the average CT attenuation values of the spleen on the three types of VNC image were also significantly lower than those on the TNC images [TNC, VNCa, VNCv, and VNCd: 58.00 (52.00–64.00) HU, 54.95 (52.78–58.68) HU, 56.00 (53.60–60.38) HU, and 55.10 (53.43–59.28) HU, respectively; P<0.05]. The average LSR on the three types of VNC image did not differ significantly from that on TNC images [TNC, VNCa, VNCv, and VNCd: 1.12±0.20, 1.11 (1.03–1.19), 1.10 (1.02–1.20), and 1.11 (1.03–1.18), respectively; P>0.05; *Table 1*]. Bland-Altman plots to evaluate the measurement agreement of the LSR between the three types of VNC image and the TNC images showed good consistency and no significant bias (*Figure 3*).

Percentages of cases with CT attenuation values with differences of less than 5 and less than 10 HU

Regarding the CT attenuation value of the liver, an intraindividual difference of less than 5 HU was observed between the TNC and three types of VNC image (VNCa, VNCv, and VNCd) in 73.13%, 73.13%, and 75.63% of cases, respectively, and an intraindividual difference of less than <10 HU was observed in 96.25%, 96.25%, and 95.63% of cases, respectively. Regarding the CT attenuation value of the spleen, an intraindividual difference of less than 5 HU was observed between the TNC and three types of VNC image (VNCa, VNCv, and VNCd) in 60.00%, 65.63%, and 63.75% of cases, respectively, and an intraindividual difference of less than 10 HU was observed

Table 1 Comparison of the computed tomography attenuation values in the TNC and the three types of VNC image

Parameter	Liver	Spleen	LSR
TNC	63.00 (57.25 to 71.75)	58.00 (52.00 to 64.00)	1.12±0.20
VNCa	61.25 (57.00 to 65.70)	54.95 (52.78 to 58.68)	1.11 (1.03 to 1.19)
VNCv	62.30 (58.50 to 66.68)	56.00 (53.60 to 60.38)	1.10 (1.02 to 1.20)
VNCd	61.70 (57.80 to 66.23)	55.10 (53.43 to 59.28)	1.11 (1.03 to 1.18)
Z/*t**	7.703	5.588	0.195
Z/*t*#	3.956	–2.471	–0.584
Z/*t*&	5.881	4.607	0.405
P value*	0.000	0.000	0.846
P value#	0.000	0.013	0.559
P value&	0.000	0.000	0.686

Data are expressed as median (interquartile range) or mean ± standard deviation. *, TNC was compared with VNCa; #, TNC was compared with VNCv; &, TNC was compared with VNCd. TNC, true non-contrast; VNC, virtual non-contrast; LSR, liver-to-spleen ratio; VNCa, virtual non-contrast from the arterial phase; VNCv, virtual non-contrast from the venous phase; VNCd, virtual non-contrast from the delayed phase.

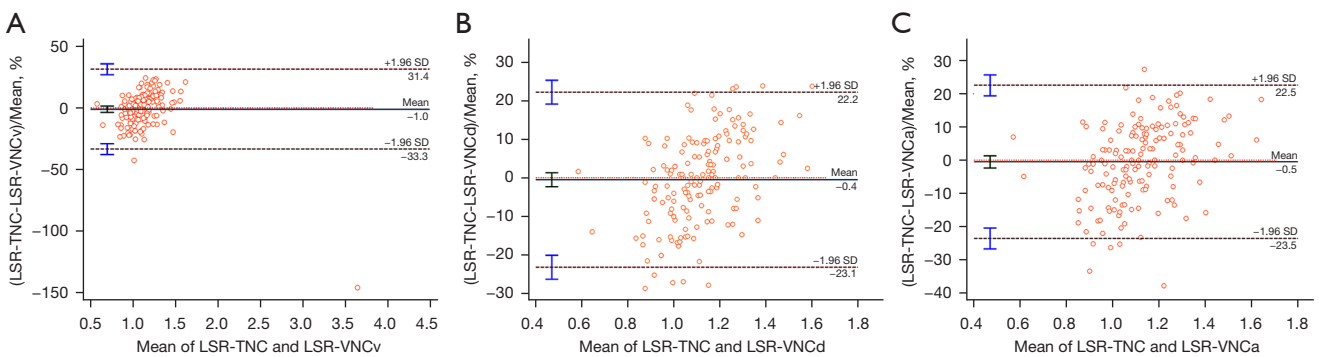

Figure 3 Bland-Altman plots evaluating the measurement agreement of the LSR between TNC and VNC images. (A) Measurement consistency of TNC and VNCv images. (B) Measurement consistency of TNC and VNCd images. (C) Measurement consistency of TNC and VNCa images. LSR, liver-to-spleen ratio; TNC, true non-contrast; VNC, virtual non-contrast; VNCa, virtual non-contrast from the arterial phase; VNCv, virtual non-contrast from the venous phase; VNCd, virtual non-contrast from the delayed phase; SD, standard deviation.

in 90.00%, 89.38%, and 90.00% of cases, respectively (*Table 2*). The violin plots in *Figure 4* show differences in the CT attenuation values of the liver and spleen between the TNC images and three types of VNC image.

Comparison of patients with and without CRFLD

In this study, there were no significant differences in age, sex, or BMI between the CRFLD and non-CRFLD groups (all P values >0.05; *Table 3*). The average CT attenuation values of the liver on TNC, VNCa, VNCv, and VNCd images were all significantly lower in the CRFLD group than in the non-CRFLD group (all P values <0.001). The average LSR was also significantly lower in the CRFLD group than in the non-CRFLD group (all P values <0.001). However, the average CT attenuation values of the spleen showed no significant difference between the two groups of patients (all P values >0.05; *Table 3*).

Performance of the LSR for diagnosing CRFLD

The AUC values of the LSR calculated on TNC, VNCa,

Table 2 The number (percentage) of cases with computed tomography attenuation values with differences of less than 5 HU and less than 10 HU between the TNC and the three types of VNC image

Organ	|TNC-VNCa|, n (%)		|TNC-VNCv|, n (%)		|TNC-VNCd|, n (%)	
	<5 HU	<10 HU	<5 HU	<10 HU	<5 HU	<10 HU
Liver	117 (73.13)	154 (96.25)	117 (73.13)	154 (96.25)	121 (75.63)	153 (95.63)
Spleen	96 (60.00)	144 (90.00)	105 (65.63)	143 (89.38)	102 (63.75)	144 (90.00)

HU, Hounsfield units; TNC, true non-contrast; VNC, virtual non-contrast; VNCa, virtual non-contrast from the arterial phase; VNCv, virtual non-contrast from the venous phase; VNCd, virtual non-contrast from the delayed phase.

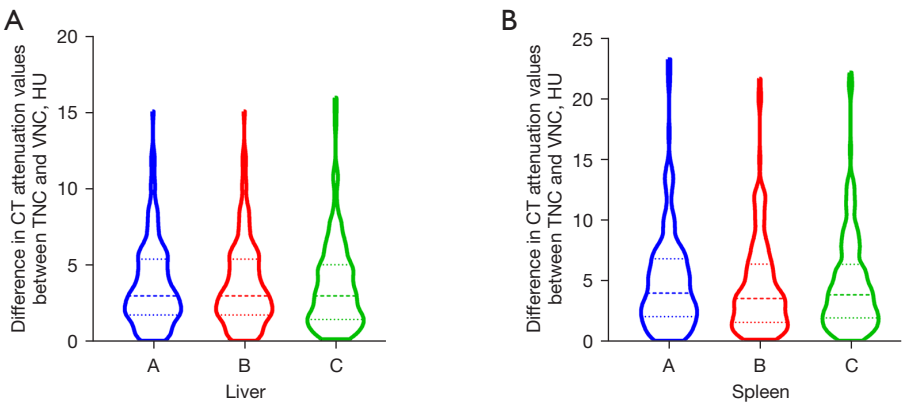

Figure 4 Violin plots summarizing the differences in the CT attenuation values between the TNC and VNC images of the liver and spleen. (A) Differences in CT attenuation values between TNC and VNC images of the liver. (B) Differences in CT attenuation values between TNC and VNC images of the spleen. A, the difference between TNC and VNCa images; B, the difference between TNC and VNCv images; C, the difference between TNC and VNCd images. CT, computed tomography; TNC, true non-contrast; VNC, virtual non-contrast; HU, Hounsfield units; VNCa, virtual non-contrast from the arterial phase; VNCv, virtual non-contrast from the venous phase; VNCd, virtual non-contrast from the delayed phase.

VNCv, and VNCd images were 0.870 (95% CI: 0.808–0.918), 0.852 (95% CI: 0.787–0.903), 0.819 (95% CI: 0.750–0.875), and 0.851 (95% CI: 0.786–0.902), respectively (*Figure 5*). These values were not significantly different when compared using the DeLong test (all P values >0.05; *Table 4*). The cutoff values for TNC, VNCa, VNCv, and VNCd images were 0.99, 1.07, 1.04, and 1.08, respectively. The sensitivity of TNC, VNCa, VNCv, and VNCd images was 80.8%, 92.3%, 76.9%, and 92.3%, respectively, and the specificity was 80.6%, 69.4%, 77.6%, and 68.7%, respectively (Table S2).

Results of subjective assessment

As shown in *Table 5*, the image quality and two reviewers' subjective ratings of diagnostic confidence did not differ significantly between the TNC and three types of VNC image (all P values >0.05).

Potential dose savings

The average values of the total DLP, CTDIvol, and ED in the contrast phase were 2,410.51±650.05 mGy·cm, 46.32±6.54 mGy, and 36.16±9.75 mSv, respectively, which were significantly higher than those in the non-contrast phase (598.37±264.89 mGy·cm, 14.66±5.32 mGy, and 8.98±3.97 mSv, respectively; all P values <0.001). Elimination of the non-contrast phase from three-phase abdominal acquisition resulted in a potential dose saving of approximately 25.0%.

Table 3 Differences in the clinical information and computed tomography attenuation values between the patients with and without CRFLD

Characteristics	Subtypes	Non-CRFLD (n=134)	CRFLD (n=26)	χ^2/Z/t	P value
Clinical information	Age, years	56.41±12.26	55.54±7.78	0.469	0.641
	Male (%)	91 (67.91)	17 (65.38)	0.063	0.821
	BMI, kg/m^2	22.44 (20.92 to 24.00)	21.66 (20.28 to 22.55)	–1.871	0.061
Liver	TNC	65.00 (59.00 to 73.00)	55.50 (49.50 to 61.25)	–5.256	0.000
	VNCa	61.90 (58.48 to 66.58)	53.90 (49.48 to 56.75)	–6.150	0.000
	VNCv	63.45 (60.40 to 67.98)	54.75 (51.93 to 58.45)	–6.085	0.000
	VNCd	62.50 (59.45 to 66.65)	55.00 (50.18 to 57.68)	–6.126	0.000
Spleen	TNC	56.50 (51.00 to 64.00)	59.00 (56.00 to 63.50)	–1.611	0.107
	VNCa	55.00 (52.68 to 58.80)	54.90 (52.90 to 58.15)	–0.405	0.686
	VNCv	55.85 (53.60 to 60.60)	56.25 (53.60 to 59.20)	–0.412	0.681
	VNCd	55.10 (53.35 to 59.30)	55.60 (53.35 to 59.33)	–0.259	0.796
LSR	TNC	1.16±0.19	0.91±0.14	8.074	0.000
	VNCa	1.13 (1.05 to 1.21)	0.97 (0.91 to 1.04)	–5.620	0.000
	VNCv	1.12 (1.05 to 1.20)	0.98 (0.89 to 1.04)	–5.097	0.000
	VNCd	1.13 (1.07 to 1.21)	1.00 (0.90 to 1.03)	–5.661	0.000

Data are expressed as median (interquartile range), mean ± standard deviation, or n (%). CRFLD, chemotherapy-related fatty liver disease; LSR, liver-to-spleen ratio; BMI, body mass index; TNC, true non-contrast; VNCa, virtual non-contrast from the arterial phase; VNCv, virtual non-contrast from the venous phase; VNCd, virtual non-contrast from the delayed phase.

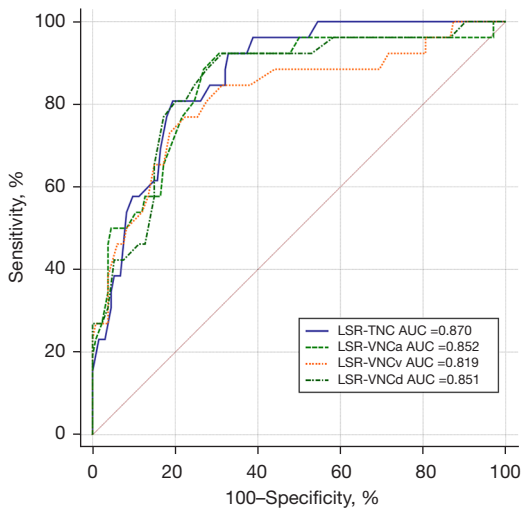

Figure 5 The performance of the LSR in diagnosing CRFLD. LSR, liver-to-spleen ratio; TNC, true non-contrast; VNCa, virtual non-contrast from the arterial phase; VNCv, virtual non-contrast from the venous phase; VNCd, virtual non-contrast from the delayed phase; AUC, area under the curve; CRFLD, chemotherapy-related fatty liver disease.

Table 4 Pairwise comparative analysis of the AUC values

Parameter in the DeLong test	Subtypes	Z value	P value
LSR-TNC	LSR-VNCa	0.384	0.701
	LSR-VNCv	0.960	0.337
	LSR-VNCd	0.432	0.666
LSR-VNCa	LSR-VNCv	1.102	0.271
	LSR-VNCd	0.036	0.972
LSR-VNCd	LSR-VNCv	1.187	0.235

AUC, area under the curve; LSR, liver-to-spleen ratio; TNC, true non-contrast; VNCa, virtual non-contrast from the arterial phase; VNCv, virtual non-contrast from the venous phase; VNCd, virtual non-contrast from the delayed phase.

Table 5 Subjective evaluation of image quality and diagnostic confidence

Group score	Reviewer 1					Reviewer 2					ICC value
	1	2	3	4	5	1	2	3	4	5	
Image quality											
TNC	0	0	0	34	126	0	0	0	31	129	0.905
VNCa	0	0	0	36	124	0	0	0	32	128	0.852
VNCv	0	0	0	35	125	0	0	0	34	126	0.834
VNCd	0	0	0	37	123	0	0	0	34	126	0.874
Z/t*			–1.414					–0.302			–
Z/t#			–1.000					–1.000			–
Z/t&			–1.732					–1.000			–
P value*			0.157					0.763			–
P value#			0.317					0.317			–
P value&			0.083					0.317			–
Diagnostic confidence											
TNC	0	0	2	42	116	0	0	1	41	118	0.901
VNCa	0	0	3	43	114	0	0	2	42	116	0.883
VNCv	0	0	2	44	114	0	0	2	43	115	0.880
VNCd	0	0	5	39	116	0	0	4	38	118	0.871
Z/t*			–1.732					–1.134			–
Z/t#			–1.414					–0.943			–
Z/t&			–1.732					–0.632			–
P value*			0.083					0.257			–
P value#			0.157					0.346			–
P value&			0.083					0.527			–

*, TNC was compared with VNCa; #, TNC was compared with VNCv; &, TNC was compared with VNCd. ICC, intra/interclass correlation coefficient; TNC, true non-contrast; VNCa, virtual non-contrast from the arterial phase; VNCv, virtual non-contrast from the venous phase; VNCd, virtual non-contrast from the delayed phase.

Discussion

This study explored whether VNC technology could serve as a replacement for TNC imaging in the diagnosis of CRFLD while reducing the radiation dose. The main findings of this study were as follows. First, the average CT attenuation value of the liver and the LSR measured on TNC and three types of VNC image were significantly lower in patients with CRFLD than in those without CRFLD. Second, the LSR showed good agreement between TNC and VNC images, with no difference in diagnostic performance observed. Finally, with VNC technology, little difference was noted in the image quality and diagnostic confidence compared to TNC imaging, while the radiation dose was reduced by approximately 25.0%.

The consistency between TNC and VNC images must be established before VNC imaging can serve as a substitute for TNC imaging in clinical practice (26). However, conflicting results have been reported by previous studies to assess the consistency of abdominal TNC and VNC images (22,27-29). Borhani *et al.* (22) and Laukamp *et al.* (27), for example, found that the average CT attenuation values of the liver or spleen did not differ significantly between TNC and VNC images. However, Haji-Momenian *et al.* (28)

reported that the CT values of the liver and spleen on VNC images were higher than those on TNC images. Conversely, in the present study, the CT values of the liver and spleen were lower on VNC images than on TNC images, which is consistent with results reported by Choi *et al.* (29). This difference in results might be because VNC images can be affected by different material decomposition algorithms, scanners, and scanning schemes, which can result in variation in the elimination of the iodine component. Thus, the standard protocol is a prerequisite for VNC technology to replace TNC imaging in clinical applications.

Although there are differences between VNC and TNC images owing to variation in the elimination of the iodine component, differences of CT attenuation value less than 10 HU are negligible (24). Ananthakrishnan *et al.* (23) reported that 48.8% and 81.4% of patients had differences of less than 5 HU and 10 HU, respectively, between TNC and VNC images of the liver, while 48.8% and 73.8% of patients had differences of less than 5 HU and 10 HU, respectively, between TNC and VNC images of the spleen. Borhani *et al.* (22) found that 18.0% and 17.0% of patients had a difference of more than 10 HU between VNC and TNC images of the liver, respectively, and 22.0% and 18.0% of patients had a difference of more than 10 HU between VNC and TNC images of the spleen, respectively. Similar to these results (22,23), our study showed that more than 85.0% of patients had a difference of less than 10 HU in the CT values of the liver and spleen between VNC and TNC images. This result can be explained because VNC, based on a multimaterial decomposition algorithm, has a slight deviation in iodine removal. Moreover, in this study, the proportion of patients with a difference of more than 10 HU between the TNC and three types of VNC image was very low, indicating a negligible difference between the VNC and TNC images. Further, we also found that the image quality was good for both VNC and TNC images, showing that the VNC technology has little impact on image quality (30). We therefore recommend the use of VNC imaging as a good substitute for TNC imaging in clinical practice, as VNC technology ensures accurate and high-quality images.

The possibility of diagnosing CRFLD is important for patients undergoing CT for cancer follow-up (3). However, the high radiation dose required for the CT examination should not be ignored (31). Therefore, we used the VNC technique to evaluate CRFLD and reduce the radiation dose. We found that there were no differences in the average CT attenuation values of the spleen on TNC or VNC images between patients with and without CRFLD. However, the average CT attenuation values of the liver and the LSR on TNC and VNC images were lower in patients with CRFLD than in those without, which was consistent with the results of previous studies on NAFLD (29). In addition, two experienced abdominal radiologists performed a subjective assessment of CRFLD on the TNC and three types of VNC image and had consistent diagnostic confidence between the two types of images. This result was expected, since the VNC technique is based on a multimaterial decomposition algorithm that removes iodine from the enhancement contrast to resemble TNC images (21-23). Additionally, similar to other studies (23,24,32), our study demonstrated that VNC imaging could reduce the radiation dose by approximately 25.0%. Thus, these findings confirm the clinical applicability of VNC imaging as an alternative to TNC imaging for the diagnosis of CRFLD and its ability to reduce the radiation dose.

Abdominal CT is widely used to diagnose NAFLD (33). For the assessment of NAFLD, the LSR is clinically considered to be an accurate CT measure (16). Therefore, the LSRs measured on TNC and VNC images were used separately to evaluate CRFLD to further explore the feasibility of replacing TNC imaging with VNC imaging for the diagnosis of CRFLD. We found no significant difference in the LSR when the TNC images and three types of VNC image were compared (P values =0.846, 0.559, and 0.686, respectively). Bland-Altman analysis also showed that the LSR had good consistency between the TNC and three types of VNC image, and no obvious deviation was found. A reasonable explanation for this result is that the LSR is a relatively constant parameter for diagnosing CRFLD. It differs from the average liver CT attenuation value, which varies based on the patient and scanning equipment parameters (34). Also, we found that the LSR calculated on the TNC and three types of VNC image showed a promising performance in diagnosing CRFLD. No significant difference was detected in the AUC values with the DeLong test. According to Choi *et al.* (29), fatty liver could be correctly diagnosed using the LSR with AUC values greater than 0.75. Therefore, the LSR measured on VNC images is a good substitute for that measured on TNC images and could serve as a credible diagnostic tool for CRFLD. Also consistent with Choi *et al.*'s (29) findings, the cutoff values of the LSR on the three types of VNC image were higher than those on the TNC images because the CT values of the spleen on the TNC and three types of VNC image differed greatly from those of the liver.

Therefore, appropriate cutoff values of the LSR should be used to indicate the possibility of CRFLD on VNC images.

There were several limitations to the study. First, it was a single-center study, and a larger multicenter study is warranted to verify our findings. Second, liver biopsy findings were not used for CRFLD evaluation. In the future, liver biopsy will be used as the gold standard to further validate the advantages of VNC imaging for CRFLD. Finally, the grade of CRFLD was not considered in this study; hence, the relationship between VNC and the grade of CRFLD needs to be further explored.

Conclusions

VNC images did not substantially differ from TNC images and had comparable image quality and diagnostic performance for CRFLD. They also enabled the radiation dose to be reduced by 25%. Therefore, VNC images are a suitable substitute for TNC images.

Acknowledgments

Funding: This work was supported by the National Natural Science Foundation of China (No. 82071872).

Footnote

Reporting Checklist: The authors have completed the STARD reporting checklist. Available at https://qims.amegroups.com/article/view/10.21037/qims-22-742/rc

Conflicts of Interest: All authors have completed the ICMJE uniform disclosure form (available at https://qims.amegroups.com/article/view/10.21037/qims-22-742/coif). The authors report that this work was supported by the National Natural Science Foundation of China (No. 82071872). The authors have no other conflicts of interest to declare.

Ethical Statement: The authors are accountable for all aspects of the work in ensuring that questions related to the accuracy or integrity of any part of the work are appropriately investigated and resolved. The study was conducted in accordance with the Declaration of Helsinki (as revised in 2013). The Ethics Committee of Lanzhou University Second Hospital approved this study (No. 2020A-284), and individual consent for this retrospective analysis was waived.

References

1. Li J, Zou B, Yeo YH, Feng Y, Xie X, Lee DH, et al. Prevalence, incidence, and outcome of non-alcoholic fatty liver disease in Asia, 1999-2019: a systematic review and meta-analysis. Lancet Gastroenterol Hepatol 2019;4:389-98.
2. Wieland AC, Mettler P, McDermott MT, Crane LA, Cicutto LC, Bambha KM. Low awareness of nonalcoholic fatty liver disease among patients at high metabolic risk. J Clin Gastroenterol 2015;49:e6-e10.
3. Yoo JJ, Lim YS, Kim MS, Lee B, Kim BY, Kim Z, Lee JE, Lee MH, Kim SG, Kim YS. Risk of fatty liver after long-term use of tamoxifen in patients with breast cancer. PLoS One 2020;15:e0236506.
4. Huang LJ, Xu YH, Fan JG. Emphasis on clinical study of heterogeneity of non-alcoholic fatty liver disease. Zhonghua Gan Zang Bing Za Zhi 2020;28:193-7.
5. Amacher DE, Chalasani N. Drug-induced hepatic steatosis. Semin Liver Dis 2014;34:205-14.
6. Zhao J, van Mierlo KMC, Gómez-Ramírez J, Kim H, Pilgrim CHC, Pessaux P, Rensen SS, van der Stok EP, Schaap FG, Soubrane O, Takamoto T, Viganò L, Winkens B, Dejong CHC, Olde Damink SWM; . Systematic review of the influence of chemotherapy-associated liver injury on outcome after partial hepatectomy for colorectal liver metastases. Br J Surg 2017;104:990-1002.
7. Paternostro R, Sieghart W, Trauner M, Pinter M. Cancer and hepatic steatosis. ESMO Open 2021;6:100185.
8. Ting Soon GS, Wee A. Liver biopsy in the quantitative assessment of liver fibrosis in nonalcoholic fatty liver disease. Indian J Pathol Microbiol 2021;64:S104-11.
9. Sumida Y, Nakajima A, Itoh Y. Limitations of liver biopsy and non-invasive diagnostic tests for the diagnosis of nonalcoholic fatty liver disease/nonalcoholic steatohepatitis. World J Gastroenterol 2014;20:475-85.
10. Bedossa P, Patel K. Biopsy and Noninvasive Methods to Assess Progression of Nonalcoholic Fatty Liver Disease.

Gastroenterology 2016;150:1811-22.e4.
11. Nelson SM, Hoskins JD, Lisanti C, Chaudhuri J. Ultrasound Fatty Liver Indicator: A Simple Tool for Differentiating Steatosis From Nonalcoholic Steatohepatitis: Validity in the Average Obese Population. J Ultrasound Med 2020;39:749-59.
12. Nguyen TN, Podkowa AS, Park TH, Miller RJ, Do MN, Oelze ML. Use of a convolutional neural network and quantitative ultrasound for diagnosis of fatty liver. Ultrasound Med Biol 2021;47:556-68.
13. Goceri E, Shah ZK, Layman R, Jiang X, Gurcan MN. Quantification of liver fat: A comprehensive review. Comput Biol Med 2016;71:174-89.
14. Huber FA, Del Grande F, Rizzo S, Guglielmi G, Guggenberger R. MRI in the assessment of adipose tissues and muscle composition: how to use it. Quant Imaging Med Surg 2020;10:1636-49.
15. Sun T, Lin X, Chen K. Evaluation of hepatic steatosis using dual-energy CT with MR comparison. Front Biosci (Landmark Ed) 2014;19:1377-85.
16. Jawahar A, Gonzalez B, Balasubramanian N, Adams W, Goldberg A. Comparison of correlations between lipid profile and different computed tomography fatty liver criteria in the setting of incidentally noted fatty liver on computed tomography examinations. Eur J Gastroenterol Hepatol 2017;29:1389-96.
17. Tsurusaki M, Sofue K, Hori M, Sasaki K, Ishii K, Murakami T, Kudo M. Dual-Energy Computed Tomography of the Liver: Uses in Clinical Practices and Applications. Diagnostics (Basel) 2021;11:161.
18. Whitebird RR, Solberg LI, Bergdall AR, López-Solano N, Smith-Bindman R. Barriers to CT Dose Optimization: The Challenge of Organizational Change. Acad Radiol 2021;28:387-92.
19. Mu D, Bai J, Chen W, Yu H, Liang J, Yin K, Li H, Qing Z, He K, Yang HY, Zhang J, Yin Y, McLellan HW, Schoepf UJ, Zhang B. Calcium Scoring at Coronary CT Angiography Using Deep Learning. Radiology 2022;302:309-16.
20. McCollough CH, Leng S, Yu L, Fletcher JG. Dual- and Multi-Energy CT: Principles, Technical Approaches, and Clinical Applications. Radiology 2015;276:637-53.
21. Dodig D, Solocki Matić T, Žuža I, Pavlović I, Miletić D, Markić D. Side-by-side evaluation of virtual non-contrast and post-contrast images improves detection of clinically significant urolithiasis on single-phase split bolus dual-energy CT urography. Br J Radiol 2021;94:20210013.
22. Borhani AA, Kulzer M, Iranpour N, Ghodadra A, Sparrow M, Furlan A, Tublin ME. Comparison of true unenhanced and virtual unenhanced (VUE) attenuation values in abdominopelvic single-source rapid kilovoltage-switching spectral CT. Abdom Radiol (NY) 2017;42:710-7.
23. Ananthakrishnan L, Rajiah P, Ahn R, Rassouli N, Xi Y, Soesbe TC, Lewis MA, Lenkinski RE, Leyendecker JR, Abbara S. Spectral detector CT-derived virtual non-contrast images: comparison of attenuation values with unenhanced CT. Abdom Radiol (NY) 2017;42:702-09.
24. Sauter AP, Muenzel D, Dangelmaier J, Braren R, Pfeiffer F, Rummeny EJ, Noël PB, Fingerle AA. Dual-layer spectral computed tomography: Virtual non-contrast in comparison to true non-contrast images. Eur J Radiol 2018;104:108-14.
25. Brady SL, Mirro AE, Moore BM, Kaufman RA. How to Appropriately Calculate Effective Dose for CT Using Either Size-Specific Dose Estimates or Dose-Length Product. AJR Am J Roentgenol 2015;204:953-8.
26. Ma G, Han D, Dang S, Yu N, Yang Q, Yang C, Jin C, Dou Y. Replacing true unenhanced imaging in renal carcinoma with virtual unenhanced images in dual-energy spectral CT: a feasibility study. Clin Radiol 2021;76:81.e21-81.e27.
27. Laukamp KR, Lennartz S, Ho V, Große Hokamp N, Zopfs D, Gupta A, Graner FP, Borggrefe J, Gilkeson R, Ramaiya N. Evaluation of the liver with virtual non-contrast: single institution study in 149 patients undergoing TAVR planning. Br J Radiol 2020;93:20190701.
28. Haji-Momenian S, Parkinson W, Khati N, Brindle K, Earls J, Zeman RK. Single-energy non-contrast hepatic steatosis criteria applied to virtual non-contrast images: is it still highly specific and positively predictive? Clin Radiol 2018;73:594.e7-94.e15.
29. Choi MH, Lee YJ, Choi YJ, Pak S. Dual-energy CT of the liver: True noncontrast vs. virtual noncontrast images derived from multiple phases for the diagnosis of fatty liver. Eur J Radiol 2021;140:109741.
30. Zhang X, Zhang G, Xu L, Bai X, Lu X, Yu S, Sun H, Jin Z. Utilisation of virtual non-contrast images and virtual mono-energetic images acquired from dual-layer spectral CT for renal cell carcinoma: image quality and radiation dose. Insights Imaging 2022;13:12.
31. Mazloumi M, Van Gompel G, Kersemans V, de Mey J, Buls N. The presence of contrast agent increases organ radiation dose in contrast-enhanced CT. Eur Radiol 2021;31:7540-49.
32. Li Y, Li Y, Jackson A, Li X, Huang N, Guo C, Zhang H. Comparison of virtual unenhanced CT images of the abdomen under different iodine flow rates. Abdom Radiol

(NY) 2017;42:312-21.
33. Lee SW, Park SH, Kim KW, Choi EK, Shin YM, Kim PN, Lee KH, Yu ES, Hwang S, Lee SG. Unenhanced CT for assessment of macrovesicular hepatic steatosis in living liver donors: comparison of visual grading with liver attenuation index. Radiology 2007;244:479-85.
34. Jawahar A, Gonzalez B, Balasubramanian N, Adams W, Goldberg A. Comparison of computed tomography hepatic steatosis criteria for identification of abnormal liver function and clinical risk factors, in incidentally noted fatty liver. Eur J Gastroenterol Hepatol 2020;32:216-21.

Cite this article as: Jing M, Sun J, Xi H, Liu Z, Zhang S, Deng L, Han T, Zhang B, Lin X, Zhou J. Abdominal virtual non-contrast images derived from energy spectrum CT to evaluate chemotherapy-related fatty liver disease. Quant Imaging Med Surg 2023;13(2):669-681. doi: 10.21037/qims-22-742

